Electronic Supplementary Material (ESI) for Chemical Communications

A Multi-pH-dependent, Single Optical Mesosensor/Captor Design of Toxic Metals

Sherif A. El-Safty,* Md. A. Shenashen

1. Materials and method

1.1. Chemicals

All materials were used as produced without further purification. The dispersible active agent (DAA), such as cetyltrimethyl ammonium bromide [CTAB, $CH_3(CH_2)_{15}(CH_3)_3N^+ \cdot Br$], anionic surfactants (ASs), such assodium dodecyle sulfate (SDS) and F108 surfactants, dodecane (C_{12}-alkane), triblock poly(ethylene oxide)-poly(propylene oxide)-poly(ethylene oxide) copolymers of Pluronic F108 ($EO_{141}PO_{44}EO_{141}$, Mav= 14.600), and tetramethylorthosilicate (TMOS), which was used as the silica source, nitrate enneahydrate ($Al(NO_3)_3 \cdot 9H_2O$) were obtained from Sigma-Aldrich Company Ltd. USA. The Hg^{2+}, Cd^{2+}, Cr^{6+}, and Fe^{3+} ion-standard solutions was obtained from Wako Company Ltd. (Osaka, Japan). The commercially available diphenylcarbazide (DPC) chromophore was purchased from Gelest, Japan. Buffer solutions of 0.2 M KCl-HCl, and CH_3COOH-CH_3-COONa were used to adjust the pH in the 1 to 6 range. A mixture of 2-(cyclohexylamino) ethane sulfonic acid (CHES), 3-morpholinopropane sulfonic acid (MOPS), and N-cyclohexyl-3-aminopropane sulfonic acid (CAPS) was used to adjust the pH in the 7 to 12 range by using 0.2 M NaOH. MOPS and CAPS were purchased from Dojindo Chemicals, Kumamoto, Japan. Chemicals and reagents like, KCl & CH_3COONa and HCl & CH_3COOH were purchased from Wako Pure Chemicals, Osaka, Japan.

2.2. Synthesis of 3D Optical mesocaptor

First, mesocage cubic Im3m aluminosilica monoliths (with Si/Al ratios of 9) fabricated by using microemulsion phases of F108 surfactant were used as scaffolds. Under typical synthesis conditions of the mesocage scaffold, the precursor solution (0.45 g of F108 surfactant, 0.225 g C_{12}- alkane, 0.9 g of TMOS, 0.128 g of $Al(NO_3)_3.9H_2O$, and 1.125 g of H_2O-HCl) was mixed and then shaken at 50 °C until it became homogeneous. The flask that contained the synthesis composition was instantly connected to the rotary evaporator (EYELA NVC-2100) at 45 °C and at a starting pressure of 1023 hPa. After evacuation for 15 min, the resulting optical gel-like aluminosilica materials acquired the shape and size of the reaction vessel. The resultant surfactant/aluminosilica solid was gently dried at room temperature for 3 h and then allowed to stand in a sealed container at 25 °C for 1 d to complete the drying process. The organic moieties were then removed by calcination at 550 °C for 7 h. Second, a combinatorial immobilization of 0.1 M ethanol solution of DAA into 0.5 g of scaffold was used to fabricate positively charged carriers. The results of our experiment show that it is impossible to control the design of mesocaptors using direct or indirect techniques of grafting DPC onto scaffolds, due to immediate elution of the $[M\text{-}DPCn]^{n+}$ complexes in acidic or basic conditions. Thus, the development of robust hybrid mesocaptor was achieved by using DAA approach.

Third, a DPC hydrophobic probe was successfully incorporated into solid DAA-modified monoliths (charge carrier surfaces). Ethanol removal was necessary and was performed by gentle vacuum at room temperature. The immobilization of the hydrophobic solution was repeated several times until the equilibrium adsorption capacity "saturation" of probe molecules was detected spectrophotometrically. Fourth, solid DAA-DPC mesocaptors were thoroughly washed with deionized water until no elution was observed. The resulting mesocaptor was dried at 65 °C for 2 h and then ground to a fine powder (100 µm) before being used for analyte detection/removal. The adsorption capacity of the probe molecules at the saturation step was determined by monitoring the probe absorbance with adsorption time in this synthesis design. However, the adsorbed amount of DPC probes into the scaffolds was estimated at 0.165 mmol/g (i.e., ~40 mg/g).

2.3. Optical recognition/removal of Multi-metal Ions

The optical recognition/removal of metal ions using the DPC-modified captor was performed by adding a mixture that contains specific concentrations of Cr^{6+} , Fe^{3+}, Hg^{2+}, and Cd^{2+} ions adjusted at pH 2.2 (using 0.2 M of KCl/HCl/H_2SO_4), 4 (using CH_3COOH-CH_3-COONa), 8 (using a mixture of CHES/MOPS), and 11 (using a mixture of MOPS/CAPS) to ~20 mg of solid captor at constant volume (100 cm^3) while being stirred. Notably, with Cr^{6+} and Fe^{3+}, a 5 ml (0.01 M) SDS was added to the batch assays of the ion-mesocaptor systems at the acidic solutions of pH ca. 2.2 and 4. After 15 min, the solid material was collected by suction through a 25 mm diameter cellulose acetate filter paper (Sibata filter holder). The collected mesocaptor was estimated qualitatively by the naked eye and quantitatively by UV-Vis spectrometry. Metal ion concentration was analyzed using ICP-MS before and after recognition by the mesocaptor. Successive measurements were performed using wide-range concentrations of standard "well-known" solutions of metal ions to ensure both accuracy and precision of the metal ion sensing systems. The calculated standard deviation of all metal ions was in the range of 0.01% to 0.05%. The UV-Vis absorption intensities of the $[M\text{-}DPC]^{n+}$ complex formed using both the standard solutions and target samples were compared to estimate the Cr^{6+}, Fe^{3+}, Hg^{2+}, and Cd^{2+} ions.

Stimulation of phosphatidylserine exposure by Mercury

The well-controlled counteraction of toxicity in the Hg^{2+}-contaminated blood indicates that the fabricated mesocaptor may be used in the inhibition of health risks associated with elevated mercury levels in blood. However, an RBC suspension (0.5%) in a Ringer solution was prepared. Hg^{2+} ions were added to the ringer in a concentration equivalent to 1 µM. After 24 h of incubation at 37 °C, with and without the mesocaptor,[19] erythrocytes were suspended in a solution comprising Annexin-V-Fluos and annexin buffer (dilution of 1:50). After 10 min of incubation, the sample was measured using flow cytometric analysis (FACS-*ICyte* from Sony). Cells were analyzed by forward scatter, and annexin-fluorescence intensity was measured in FL-1 with an excitation wavelength of 488 nm and an emission wavelength of 530 nm. Furthermore, the sample was analyzed under a fluorescence microscope (Olympus BX53, Japan, with excitation wavelength of 460 nm to 495 nm). Digital images were taken with a camera (Shimadzu,

Japan). *Motic image Pluse 2* was used to process the images.

Hemolysis Assay

A hemolysis test was performed with additional [3 μM] Hg^{2+} ions to further verify the potential of the mesocaptor in the removal of Hg^{2+} ions from a physiological system such as human blood. Mercury ions are known for their rapid interaction with sulfhydryl groups in the RBC membrane leading to membrane lipid peroxidation and eventually to cellular lysis. The hemolysis test involved a 12-hour incubation to assure significant inhibition of the Hg^{2+} ion-toxicity in RBCs using 0.02% captor. The RBC hemolysis was determined by measuring the absorbance of hemoglobin released at 540 nm (≥ 10 times). Each experiment was repeated three times on three different days. Statistical analysis was performed using the Student's t-test (SigmaPlot 11.0, at probability $p < 0.05$).

In typical experiment, the RBC suspension was incubated with a 0.02% (w/v) capturing agent in PBS, to which $HgCl_2$ in isotonic solution (0.9% NaCl) was added at a concentration of 3 μM. The mixture was incubated at 37 °C with gentle shaking for 12 h. To test whether the sensor inhibited mercury-induced hemolysis, the sample was centrifuged for 5 min at 600 g, after which the absorbance of hemoglobin at a wavelength of 540 nm was measured (iMark microplate reader Bio-Rad). Hb was released in the supernatant because of the mercury-induced hemolysis.

$$\%\ \text{of Hemolysis} = \frac{\text{Absorbance of sample} - \text{Absorbance of Blank}}{\text{Absorbance of} + \text{ve Control (H2O)} - \text{Absorbance of Blank}}\ \text{X } 100$$

Characterization Analyses

The metal ion concentration was determined using a PerkinElmer Elan-6000 Inductively Coupled Plasma Atomic Emission Spectrometer (ICP-MS). The reflectance spectrum of the solid mesocaptor was recorded using UV-Visible spectrometer (Shimadzu 3150, Japan).

Transmission electron microscopy (TEM), three-dimensional TEM surfaces (3D TEM) scanning transmission electron microscope (STEM) and dispersive X-ray analysis for elemental mapping (STEM-EDS) were characterized (JEOL, JEM model 2100F microscope). The TEM was operated by applying an acceleration voltage of 200 kV to obtain a lattice resolution of 0.1 nm and the spherical aberration of 1.0 mm. The STEM and STEM-EDS were operated at a camera length of 40 and a spot size of 1 nm. The TEM and STEM images were recorded using a CCD camera. Fourier transform diffractograms (FTD) were recorded by a slow scan charge-coupled device (CCD) camera (Gatan Model 694).

Small angle X-ray scattering (SAXS) experiments were performed at room temperature. A two-dimensional (2D) confocal mirror (Rigaku Nanoviewer) and a pinhole collimator were used to obtain a focused high flux/high transmission; a monochromatic X-ray beam of CuKα radiation ($\lambda = 1.54$ Å) was also used. The 2D SAXS patterns were recorded using a 2D detector (BrukerHi-Star) covering a range of momentum transfer $q = (4\pi/\lambda)\ sin(2\theta/2)$, from 0.2 to 10 cm^{-1}, where λ is the wavelength of the incident X-ray beam and 2θ is the scattering angle. The value of inter-particle distance (center to center) was calculated from $d = 2\pi / q_{max}$.

The textural surface properties of the mesoporous core/double shell spheres including the specific surface area and the pore structure were determined by N_2 adsorption-desorption isotherms which were measured using a BELSORP MIN-II analyzer (JP. BEL Co. Ltd) at 77 K. The pore size distribution was determined from the adsorption isotherms by using Barrett-Joyner-Halenda (BJH) method. Specific surface area (S_{BET}) was calculated using multi-point adsorption data from linear segment of the N_2 adsorption isotherms using Brunauer-Emmett-Teller (BET) theory. Before the N_2 isothermal analysis, all samples were pre-treated at 300 ^oC for 8 h under vacuum until the pressure was equilibrated to 10^{-3} Torr.

^{29}Si MAS NMR (^{29}SiMagic-angle spinning nuclear magnetic spectroscopy) spectra were measured using a Bruker AMX-500 spectrometer. The samples were placed in a zirconia sample tube 7mm in diameter.

Fourier transform infrared spectra (FTIR) were recorded by using an FTIR Prestige-21 (Shimadzu, Japan). Zeta potential of the charged surface particles was recorded by using a ZETA-READER-Mark 21. Thermogravimetric and differential thermal analyses (TG and DTA, respectively) were measured using a simultaneous DTA-TG Apparatus TG-60 (Shimadzu, Japan).

^{27}Al Magic-angle spinning nuclear magnetic spectroscopy (^{27}Al MAS NMR) was also recorded using a Bruker AMX-500 spectrometer. ^{27}Al NMR spectra were measured at a frequency of 125.78 MHz with a 90^o pulse length of 4.7 μs. For all samples, the repetition delay was 64 s with a rotor spinning at 4 kHz for ^{27}Al NMR. The chemical shift scale was externally adjusted to be zero for ^{27}Al signal by using aqueous solution (1 N) of $Al(NO_3)_3$. To investigate the acidic properties of aluminosilica samples, NH_3 temperature-programmed desorption (NH_3-TPD) was measured by using a BEL-Japan TPD-1S system with a quadrupole mass spectrometer.

To investigate the acidic properties of aluminosilica membranes, NH_3 temperature-programmed desorption (NH_3-TPD) was measured by using a BEL-Japan TPD-1S system with a quadrupole mass spectrometer.

Surface acidity of guest-free scaffolds

^{27}Al NMR and NH_3-TPD were measured to confirm the surface acidity of the guest-free samples (Figs. S1A and S1B). The ^{27}Al NMR spectra exhibited a four-coordinated resonance (Al^{IV}, AlO_4, framework) of approximately -1 ppm and an octahedral-coordinated (Al^{VI}, AlO_6,) aluminum of approximately -1 and 45 ppm. The formation of the coordination states of the aluminum species in four- and six-coordinate environments indicated the existence of different bonds among Al, O, and H. The coordination and location of aluminum sites in the frameworks were key determinants of the surface acidity of carriers, thus facilitating the creation of strong interactions between Al-OH or Si-OH surfaces and organic moieties during the stable mesocaptor fabrication. The NH_3-TPD results showed two main peaks of NH_3 desorption at approximately 200 °C and a small broad peak at 200 °C to 500 °C, indicating the formation of weak "Lewis" and mildly strong "Bronsted" acid sites of the aluminosilica OH-groups (Fig. S1B). The peaks at approximately 100 °C to 500 °C were deconvoluted using a Gaussian function, with temperature as the variant, to determine quantitatively the number and the strength of the acid sites. The number of acid sites formed interaction sites for DAA and DPC molecules, resulting in the potential stability of the mesocaptor during the sensing and removal of metal ions in acidic medium.

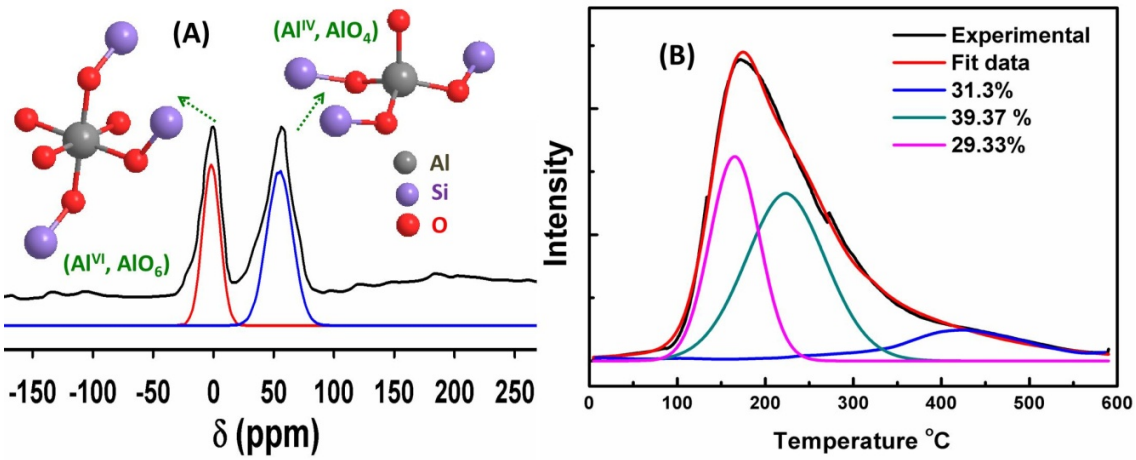

Fig. S1 NH_3-TPD (A) and ^{27}Al MAS NMR (B) spectra and deconvolution of each peak of cubic Fm3m aluminosilicate metal ion-optical mesocaptor. Inserts (A) are the octahedrally coordinated aluminum (i.e., Al^{VI}, AlO_6,) and the tetrahedral aluminum (i.e., Al^{IV}, AlO_4, and framework) at resonance -1 and 45 ppm, respectively.

The loading capacity of the immobilized DAA and DPC chelate moieties onto surface carriers was revealed through thermal and spectroscopic techniques. The TG curves revealed that the DAA and DPC chelate moieties (Fig. S2) decreased in terms of mass at approximately 180 °C to 650 °C. This decrease was accompanied by the appearance of exothermic peaks in the corresponding DTA curves, indicating the decomposition of organic components. For example, the decrease in DAA and DPC chelate moieties were 20.35 and 30.48 mass%, respectively, coinciding with the adsorption capacity (X, 0.08 mmol/L) of the loaded organic moieties of these materials. The TG analyses were consistent with the elemental content results of the EDS X-ray microanalysis of C, H, N, and O. Based on the elemental analyses (Fig. S2), the composition of CHNO in DA-CSs- and DPC-modified carriers and captor was 20.35 and 30.48 mass%, respectively.

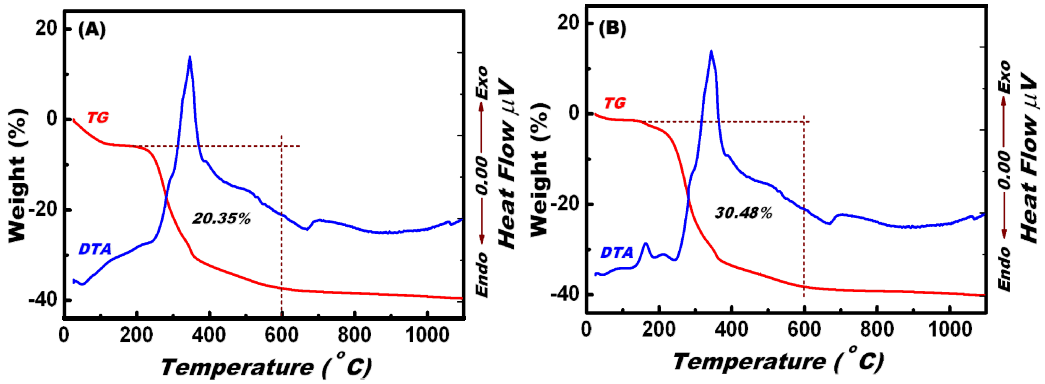

Fig. S2 TGA and DTA analyses of DA-CSs-modified-aluminosilicate carriers (A) and DAA-DPC-modified-aluminosilicate mesocaptor (B).

The FTIR spectra (Fig. S3) revealed a broad absorption band in the 3000 cm^{-1} to 3500 cm^{-1} region, indicating the presence of Si-OH asymmetric stretching for the aluminosilica monoliths, DAA- and DPC-modified carriers, and captor samples. In addition, three defined bands at 1250, 1100, and 960 cm^{-1} were assigned to the Si-O-Al, Si-O-Si, and Si-OH stretching vibrations, respectively.[1] The aluminosilica-modified DA-CSs surfactant showed additional absorption bands at 2960 and 1400 cm^{-1} because of the aliphatic C-H and stronger C-N bonds, respectively.[2] No significant changes were observed in these absorption bands after DPC chelate addition, indicating the stability of the metal ion-optical captor systems.

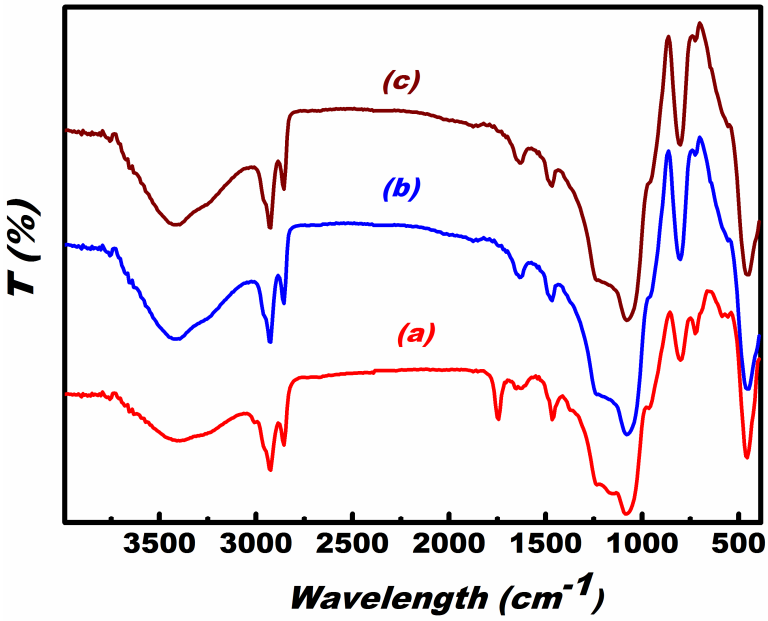

Fig. S3 FTIR characteristics of 3D aluminosilicate monoliths (a), DA-CSs-modified-aluminosilicate carriers (b), and DA-CSs-DPC-modified-aluminosilicate nanocaptor of metal ions (c).

References

1) Y. Xu, J. Zhou, G. Wang, J. Zhou, G. Tao, Anal. Chim. Acta, **2007,** 584, 204.
2) Y-Q. Weng, Y-L. Teng, F. Yue, Y-R. Zhong, B-H. Ye, Inorg. Chem. Commun. **2007**, 10, 443.

The zeta potential studies of the aluminosilica monoliths revealed an increase in the surface polarity of the charged DAA modified carriers, as evidenced by the high zeta potential values during the dense immobilization of DAA moieties (Fig. S4A). The decrease in the zeta potential with the addition of hydrophilic DPC molecules to the DAA modified carriers indicated the induced fit inhibition of surface polarity. This inhibition resulted from the ligand-to-ligand "DPC-to-DAA" interactions (Fig. S4A). Such integral interactions (i.e., van der Waals and H-bonding interactions) aid in the attraction or adsorption of DPC molecules during dense immobilization and in the attainment of the specific activity of the probe functional group "electron acceptor/donor strength" around the open DPC cavities. These open cavities are called metal ion-hostage pockets (see Scheme 1).

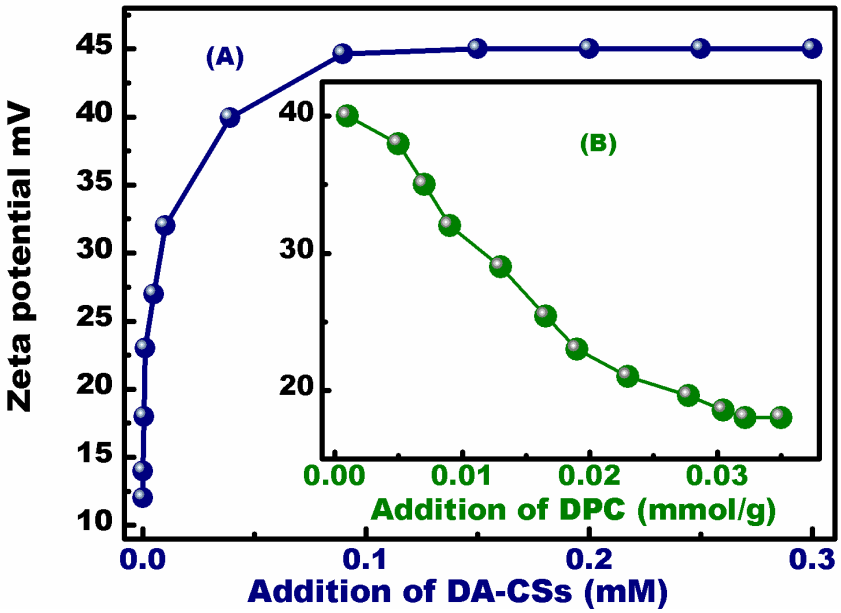

Fig. S4 Zeta potential study of aluminosilica scaffolds with surface modification by DAA concentration (A) and DPC probe concentration during the formation of DA-CSs-modified-aluminosilicate carriers (A) and DAA-DPC-modified-aluminosilicate mesocaptor of metal ions (B).

The atom-formation morphology and EDS mapping of the metal ion-optical mesocaptors were further characterized using bright-field STEM and STEM-EDS, as shown in Figs. S5A to S5G. STEM-EDS mapping was performed to characterize the surface composition and the atomic distribution of the metal ion-optical mesocaptors. The STEM-EDS map of the aluminosilica mesocaptor exhibited the presence of Si, Al, O, C, and N (Figs. S5D to S5F). However, the contributions of O, Si, and Al were mainly from the mesostructure platforms (Figs. S5a to S5d), whereas those of N and C were originally from DAA (Figs. S5e and S5f). The STEM-EDS mapping also indicated that the C and N atoms were uniformly distributed in the optical mesocaptor, thus facilitating the homogenous diffusion of metal ion into the binding sites.

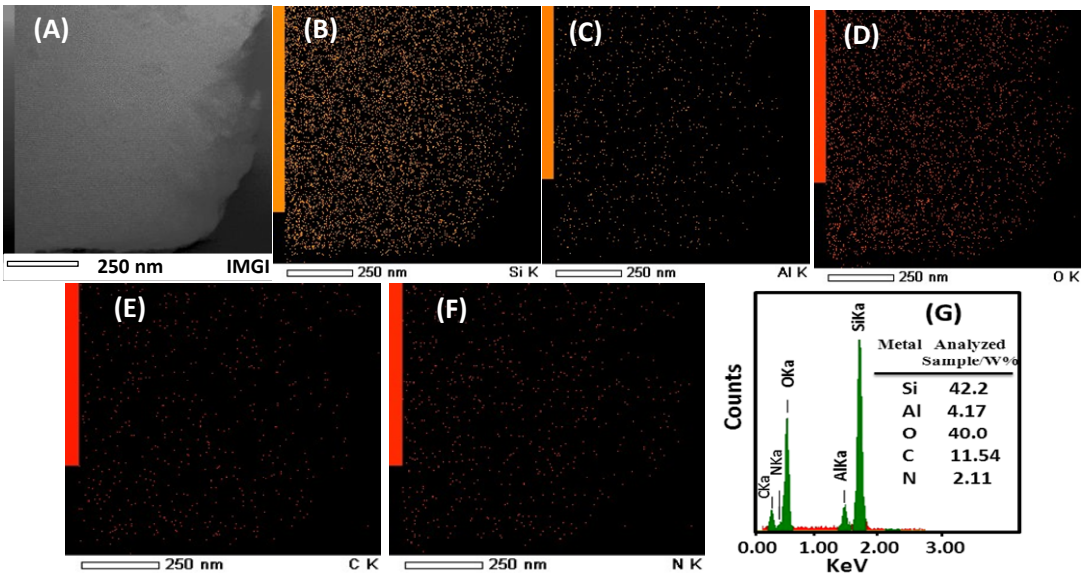

Fig. S5 STEM image and STEM-EDS mapping of the mesoporous aluminosilicate captor that was fabricated with Si/Al ratio of 9 (A) STEM image, (B) silicon, (C) aluminum, (D) oxygen, (E) carbon, (F) nitrogen, (G) EDS analysis, and the calculated values of the atomic abundance of the species present in the solid mesocaptor.

The SAXS patterns (Fig. S6A) showed finely resolved Bragg diffraction peaks, a characteristic of the cubic Fm3m aluminosilica carrier (Fig. S6A-a). The key feature in this pattern was that the design of the optical mesocaptor based on densely patterned DAA and DPC organic moieties neither changed the 3D pore geometries nor led to a significant collapse in the mesoscopically oriented ordered framework, despite the high loading of organic moieties onto the surface (Fig. S6A-b) and the sensing/capture reuse cycles (Fig. S6A-c), which are consistent with the N_2 isotherms (Fig. S6B). The N_2 isotherms (Fig. S6B) showed hysteresis loops and well-defined isotherm steepness, cage-like materials with large surface areas, and pore volumes, which also characterize mesocaptor monoliths and indicate the facile diffusion and accessibility of the metaltowards the DPC molecule.[14–16] However, the hysteresis loop width negligibly decreased with the embedding of organic moieties, indicating a slight decrease in nanoscale pore size with the fabricated nanocaptor. The characterization analysis of the mesocaptor revealed two key features as follows:

(1) Although the N_2 isothermal data indicated that organic moieties may be incorporated into inner pores, a significant amount of organic moieties was mainly anchored on pore surfaces, resulting in the high flux and rapid diffusion of the analytes.

(2) Uniformly shaped pore geometries and textural properties of worm-like and ordered nanocaptors were achieved. Such retention in structural integrity facilitates a rational design of the optical chemocaptor.

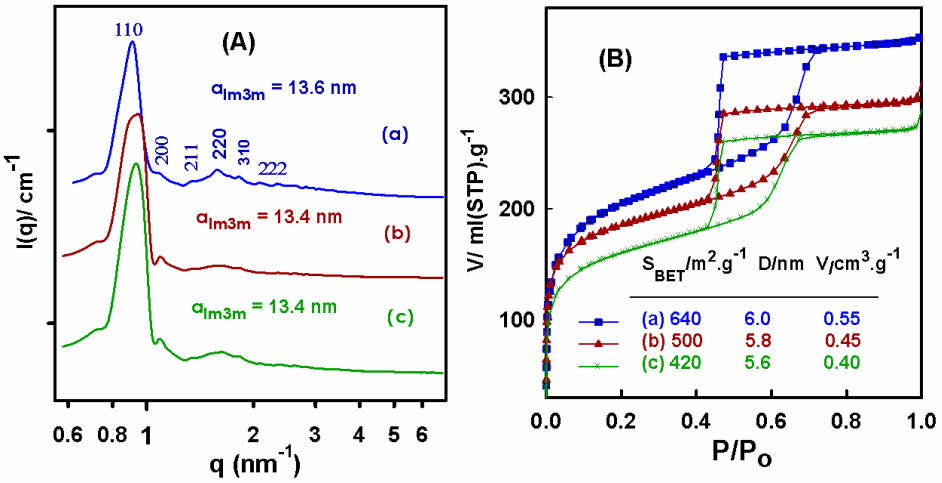

Fig. S6 SAXS patterns (A) and N_2 adsorption/desorption isotherms at 77 K (B) of the highly ordered cubic Im3m aluminosilicate with Si/Al ratio of 9 (a), metal ion-optical aluminosilicate nanocaptor (b), and after reuse cycles (c). Insert (B) lists the physical characteristics of the solid materials.

The signaling change in the reflectance spectra of the chemo-meso-captor was monitored during the formation of $[M^{+n}\text{-DPC}]^{+}$ complexes (**Fig. S7**). The reflectance spectra of the $[M^{+n}\text{-DPC}]^{+n}$ complex was observed at λ_{max} of 550, 515, 542, and 530 nm for Cr(VI), Fe(III), Hg(II), and Cd(II), respectively, as a result of the uptake of M^{+n} target ions with the DPC-captor ligand (Fig. S7). The charge-transfer reflection band of the complex was based on the ligand-binding affinity with central metal ions during the recognition and on the nature of the complex formation under specific sensing conditions. Moreover, the color change provided a simple procedure for the sensitive, selective detection of M^{+n} ions without the need for sophisticated instruments (Fig. S7).[17,18] The rapid click sensing and the flexible M^{+n}-to-DPC binding events with the formed complexes onto the organized nanocaptor resulted in the separation and preconcentration of M^{+n} ions even at a trace concentration level.

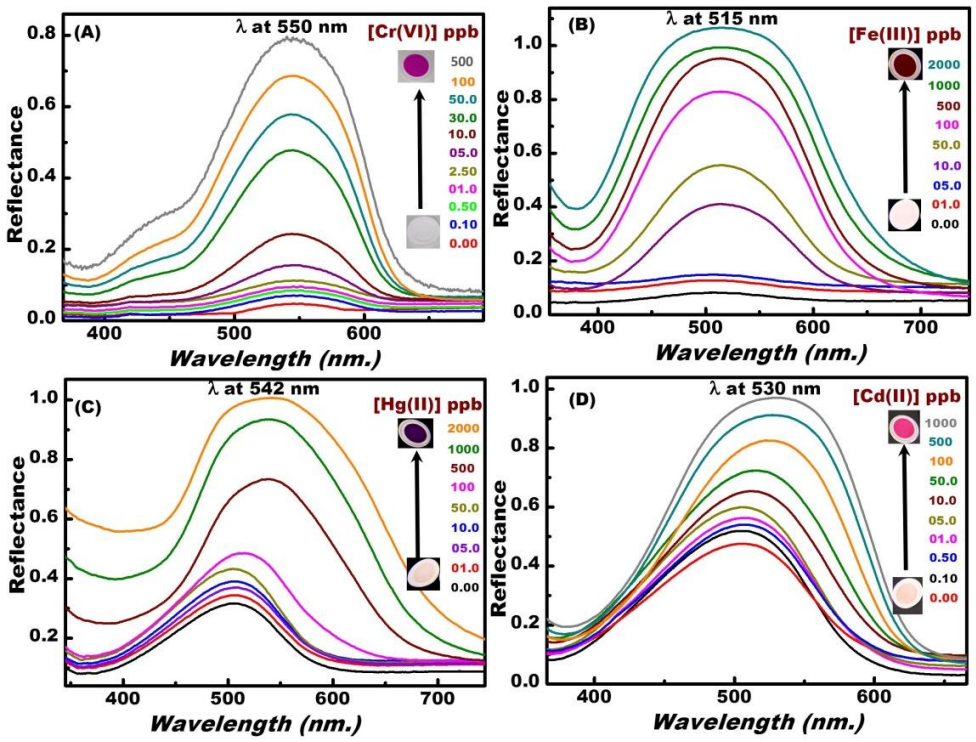

Fig. S7

Concentration-dependent changes in the UV-Vis reflectance spectra of (20 mg/L) the Cr^{6+}, Fe^{3+}, Hg^{2+}, and Cd^{2+} ion-captor system at pH 2.2, 4, 8, and 11, respectively, with a response time of 15 min and temperature of 25 °C.

To control the accurate recognition and signaling abilities of M^{+n} analyte species for ion-sensing purposes, the calibration of the click sensing method of the chemo-meso-captor was crucial. The calibration plots generally showed a linear correlation at low concentration ranges of M^{+n} analyte ions (Fig. S8). The linear curves indicated that the analytes can be removed with high efficiency over a wide-range of concentrations. Several quantification measurements (≥ 10

times) were performed using wide-range concentrations of the standard "well-known" solutions of metal ions at specific sensing conditions. The limit of detection (*LOD*) and detection range (*DR*) of M^{+n} ions was estimated from the linear part of the calibration plot by using the chemo-meso-captor (Fig. S8) according to the equation $LOD = kS_b/m$, where $k = 3$, S_b is the standard deviation for the control, and m is the slope of the calibration graph in the linear range.[16] The *DR* signified the precise correlation of our experimental sensing procedure of M^{+n} ion-sensing data obtained from the fabricated nanocaptor. The linear correlation at low concentration ranges indicated that the M^{+n} ions can be detected and then removed with high sensitivity over a wide range of concentrations. However, a nonlinear correlation at the inflection point was evident at the highest concentration of M^{+n} ions, indicating that highly efficient removal and sensitivity could be achieved at low concentrations of M^{+n} ions. In fact, with the heterogeneous workability of the optical captor/sensor, there is a limitation to determine the reflectance signal using UV-Vis-NIR machine of the high-concentration of metal ions loaded mount-probe solid surfaces. This difficulty might lead to the appearance of the saturation step at slightly high concentration of target ions (Fig. S8, insert). The capability of our nanocaptor assays, which are the first to achieve the sensitive, optical removal of nanomolar concentrations of M^{+n} ions, was shown by the LOD values (52.28×10^{-9}, 40.77×10^{-9}, 21.51×10^{-9}, and 20.34×10^{-9} mol/dm^3 for Cr^{6+}, Fe^{3+}, Hg^{2+}, and Cd^{2+} ions, respectively), which indicated that the ordered mesocaptor enabled a better recognition of M^{+n} ions.

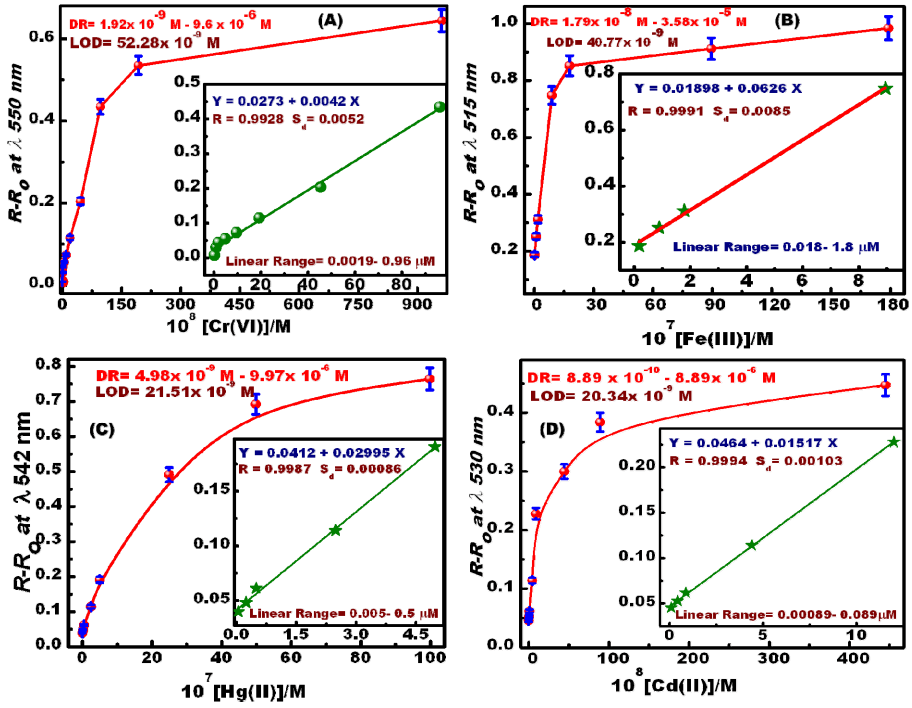

Fig. S8 Calibration curve of (20 mg/L) Cr^{6+}, Fe^{3+}, Hg^{2+}, and Cd^{2+} ion-captor system at pH 2.2, 4, 8, and 11, respectively, at temperature of 25 °C.

The selectivity of the Cr^{6+}, Fe^{3+}, Hg^{2+}, and Cd^{2+} ion sensor/captor over the active multicomponent ions and species was examined. However, in real samples, the Cr^{6+}, Fe^{3+}, Hg^{2+}, and Cd^{2+} ions are normally encapsulated by a variety of matrix compounds (Fig. 3 and Supplementary S9). Results from both selectivity profiles of the mesocaptor showed that [1000 ppm] alkali and alkaline-earth metal (i.e., Na^{+}, Cs^{+}, Li^{+}, Mg^{2+}, and Ca^{2+} ions) did not practically interfere. With the addition of an equivalent amount of transition metal ions (such as Cu^{2+}, Ni^{2+}, Co^{2+}, Pb^{2+}, and Zn^{2+}) to Cr^{6+}, Fe^{3+}, Hg^{2+}, and Cd^{2+} ion-captor systems, a slight disturbance (±3%) in the quantitative determination and removal of target ions was evident, particularly at pH 2.2, 4, 8, and 11. However, with the addition of high-doses of these competitive elements, the addition of a mixture of 0.15 mM of citrate, thiosulphate, and tartrate to the sensing/removal assays was necessary to enhance the matrix tolerance concentrations by up to a 100-fold excess over Cr^{6+}, Fe^{3+}, Hg^{2+}, and Cd^{2+} target ions. The metal ions of the lanthanide series were absolutely non-competent for the DPC-modified captor. Other heavy metal ions, such as Mo^{3+}, Bi^{3+}, and Sb^{3+}, did not interfere in the DPC-modified captor, even with a tolerance of up to a 100-fold excess over target ions. Interestingly, in each target ion-captor system at an acidic or basic media, the other three-ion targets should be eliminated from the solution using 0.2 mM thiosulphate and thiocyanide because of the high interference effect.
Furthermore, the organic acids and surfactants and inorganic anions that might impede the sensing/capture process showed no significant effect on the DPC-modified captor with tolerance concentrations of up to a 20-fold excess over Cr^{6+}, Fe^{3+}, Hg^{2+}, and Cd^{2+} target ions. In fact, the selectivity of the nanosensors for Cr^{6+}, Fe^{3+}, Hg^{2+}, and Cd^{2+} target ions over active multicomponent ions and species (Fig. 3 and S9) indicated the high thermodynamic binding of target ions for N- and O-chelate DPC ligand and the strong M-to-DPC binding at the optimized pH of 2.2, 4, 8, and 11.

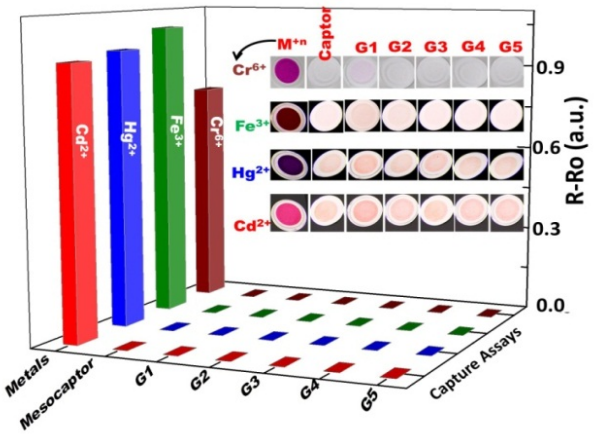

Fig. S9 Effect of the additive anions as interference ions on the signaling spectra at 550, 515, 542, and 530 nm, recorded with (20 mg/L) ion-captor at pH 2.2, 4, 8, and 11, respectively (Ro), and with the addition of metals, such as [500 ppb] Cr^{6+}, Fe^{3+}, Hg^{2+}, and Cd^{2+} ions (R), at a temperature of 25 °C. Note: the interfered [10 ppm] anions from the five groups are as follows: G1 (CTAB, Triton X, $C_8H_4O^{4-}$), G2 ($C_6H_5O_7^{3-}$, $C_2O_4^{2-}$), G3 (CH_3COO^{-}, NO_2^{-}), G4 (NO_3^{-}, SO_3^{2-}), and G5 (SO_4^{2-}, CO_3^{2-}, PO_4^{3-}).

Adsorption uptake of metal ions using chemo-meso-captors in real samples

To test the practical implementation of the mesocaptor design, we performed the adsorption process of target metals from naturally occurring environmental fluids at specific pH-dependent conditions and at a temperature of 25 °C. ICP-MS analysis was used to identify and to determine the concentrations of the various constituents. ICP data indicated that the natural samples contained approximately 15.7 mg dm^{-3} to 265 mg dm^{-3} of alkali and alkaline earth metal ions, in addition to traces of Mn^{2+}, Sb^{3+}, and Sn^{2+} ions (0.02 mg dm^{-3} to 0.083 mg dm^{-3}). In these samples, various concentrations of Cr^{6+}, Fe^{3+}, Hg^{2+}, and Cd^{2+} ions (in the range of 0.001 mg dm^{-3} to 2.0 mg dm^{-3}) were spiked. To verify the efficient adsorption behavior of DPC-mesocaptor in terms of the loading capacity and efficient binding at the ultra-trace level of M^{+n} concentrations, we applied the Langmuir isotherms (Figs. S10A to S10D) according to the following equation:[17,18]

$$C_e/q_e = 1/(K_L q_m) + (1/q_m)C_e$$

where q_m ($mg.g^{-1}$) is the amount of metal ions removed to form a monolayer coverage, and K_L is the Langmuir adsorption equilibrium constant. The monolayer coverage can be obtained from a plot of C_e/q_e versus C_e (Figs. S10a to S10d), which gives a straight line.

The linear adsorption curves indicated two key components: (1) a wide range of concentrations of metal ions can be removed in a one-step treatment and (2) the formation of the monolayer coverage of the metal ions in the interior pore surfaces of mesoporous aluminosilica captors with these removal system assays. The practical adsorption capacity q_m and the Langmuir coverage constant K_L were obtained from the slope and the intercept of the linear plot. The linear removal curves indicated that a wide range of metal ion concentrations can be removed from aqueous water in a one-step treatment with high adsorption efficiency of ~94% to ~96%. These results indicated that the practical removal of 1 g of Cr(VI) , Fe(III), Hg(II), and Cd(II) ions from an aqueous solution required ~4.11, 6.59, 4.07, and 8.54 g of nanocaptors, respectively.

Our nanocaptors displayed a significant adsorption efficiency over commercial adsorbents (such as nanoporous silica, activated carbons, sphagnum moss peat, TiO_2, coconut shell charcoal, and ion-exchange resins), which also require intensive design and experimental conditions during the adsorption and assessment monitoring of metal ions.[18] Indeed, 3D architectures with uniform pores of chemo-mesocaptors not only facilitate a high loading capacity of analytes, but also create visual removal and sensing recognition systems for these toxic metal ions from the aqueous solution.[18]

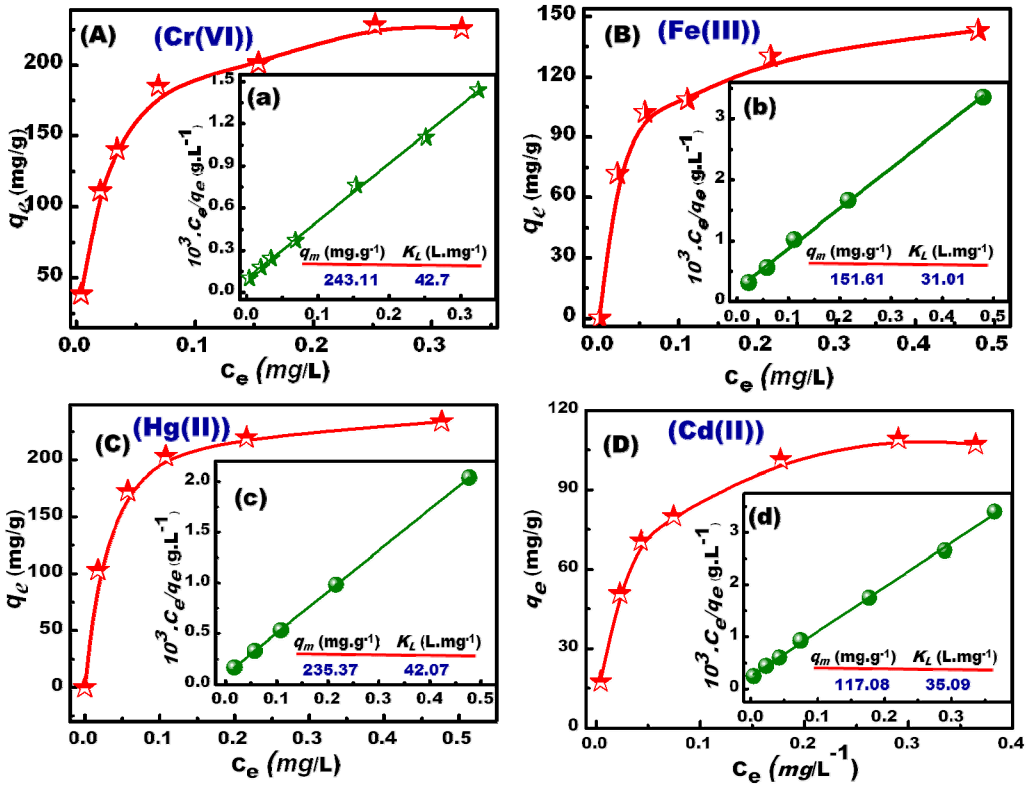

Fig. S10 Langmuir adsorption isotherms and the liner plots (inserts) of the removal processes of Cr^{6+}, Fe^{3+}, Hg^{2+}, and Cd^{2+} ions using the DPC-modified-aluminosilica captor at pH 2.2, 4, 8, and 11, respectively, and at a temperature of 25 °C.

Multi-metal mesocaptor reusability & waste-management control

From a waste management point of view, toxicity control and the collection of the captured pollutant species with consistent solid captor fidelity are highly important.[18] In this study, acetic acid, HCl, and EDTA reagents were used as the stripping agents for the effective extraction and collection of Cr^{6+}, Fe^{3+}, Hg^{2+}, and Cd^{2+} ions from mesocaptor surfaces after the adsorption process (i.e., decomplexation). For example, a 0.2 $mol.L^{-1}$ concentration of acetic acid was used as a stripping agent for the extraction and collection of of Cr^{6+} ions. Stripping experiments were conducted several times via a liquid-exchange process to release the metal ions and to obtain "metal ion-free" captor surfaces. After a few minutes, the $[M\text{-}DPCn]^{+n}$ captor returned to its initial color, indicating the release of the metal ions from the solid captor. The reflectance spectra of the solid captor displayed spectra similar to those of the freshly fabricated DPC- captor, indicating the stability of the captor. The ICP-MS analysis of the collected target metal solution also indicated that 95.1% to 99.4% of the target metal ions can be released using this simple chemical treatment.

A major advantage of the mesocaptor is its retaining functionality in terms of metal ions recovery after multiple reuse cycles.[15-17] The signal intensity of the captor with each reuse cycle was compared with the signal spectra of the captor prior to the use of the stripping agent. The captor had well-controlled signalling in the recovery of M^{+n} ions even after multiple reuse cycles (that is, ≥ 7) (Fig. S9A). On the other hand, the time required for capturing metal ions onto the DPC-modified captor after six recycling processes slightly increased to ~20 min. The functional molecular probe onto mesocaptors generally attained the electron acceptor/donor strength functionality to achieve effective binding and signalling of the metal ion targets despite substantial influence upon cycling.

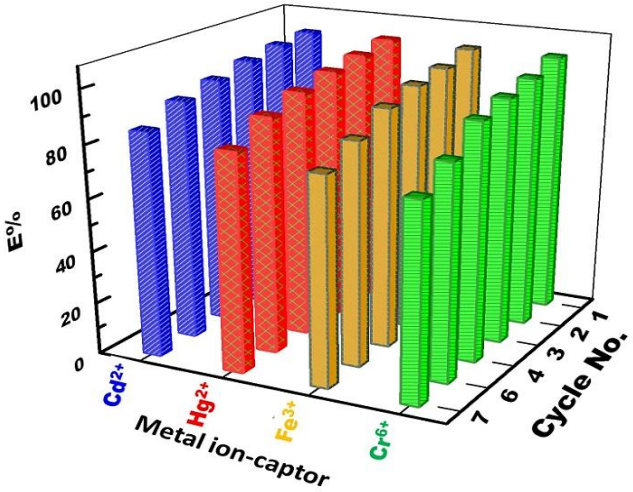

Fig. S11 Evaluation of the efficiency changes for the recognition and capturing properties of [0.5 ppm] Cr^{6+}, Fe^{3+}, Hg^{2+}, and Cd^{2+} ions using (20 mg/L) DPC-modified mesocaptor after seven regeneration/reuse cycles at 25 °C.

To explore the removal of mercury ions from a physiological solution, a suspension of RBCs was prepared to illustrate the bioapplicability of the sensor. The effects of the counteraction of phosphatidylserine (Ptd-L-Ser) receptor exposure were also investigated to further illustrate the inhibition of the mercury ion-toxicity in RBCs using the sensor. In the experimental assay, the Ptd-L-Ser receptor was exposed to the outer surface of the RBC membrane over the incubation (24 hrs) with 1 μM of Hg^{2+} ions.[19] The addition of Annexin-V-Fluos to the incubated RBCs resulted in green fluorescence due to the interaction of the Annexin-V-Fluos with exposed Ptd-L-Ser receptors on the RBC membrane. This interaction was measured using flow cytometric analysis (Icyte-Sony) (Fig. S12A, ESI†) and examined under a fluorescent microscope (Fig. S12B-E, ESI†). The percentages of Annexin binding cells and green fluorescence were considered as indicators of Hg^{2+}-induced toxicity in RBCs (Fig. S12, ESI†). The overlay histogram (Fig. S12A, ESI†) shows no Annexin binding cells with the incubation assays (RBCs–Hg^{2+}–captor), indicating that there is neither Ptd-L-Ser receptor exposure nor green fluorescence (Fig. S12D, ESI†). Similarly, the incubation with sensor/captor alone consistently exhibited almost no green fluorescence when interacting with Annexin-V-Fluos, as shown by (Fig. 12B and E, ESI†). These results indicate the inhibition of Hg^{2+} ion toxicity via the significant removal of a low-level Hg^{2+} toxicant, suggesting higher flux and diffusion of Hg2+ ion-transport into the captor than into the RBC membranes. A hemolysis test was also performed with additional [3 μM] Hg^{2+} ions (Fig. S12F, ESI†).[19] Results show that the mercury-induced hemolysis significantly decreased after the addition of the captor. This inhibition is the key to establishing the sensor design as the ideal method of the counteraction and neutralization of Hg^{2+}-stimulated hemolysis via the removal of Hg^{2+} ions.

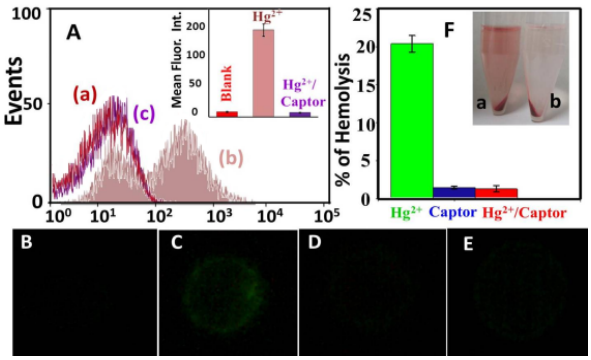

Fig. S12. (A) Histogram of annexin binding RBCs incubated for 24 hours with (a) blank, (b) 1μM Hg^{2+}, (c) 1μM Hg^{2+}/Captor. (A, Insert) mean fluorescence intensity of annexin-V binding for erythrocytes incubated with 1μM Hg^{2+}, blank, and Hg^{2+}/captor. Error bars represent Standard Error of Mean (SEM). Fluorescence images (100X) of RBCs (Annexin-V Fluos) incubated for 24 hours with (B) blank, (C) Hg^{2+}, (D) Hg^{+2}/ captor, and (E) nanocaptor alone under excitation wavelengths of 460 to 495 nm (Scale-bar: 10 μm). (F) Percentage of hemolysis resulting from the incubation of 3 μM mercury using RBC suspension, and hemolysis inhibition due to the removal of Hg^{2+} by the captor. The error bars represent SEM, (F, insert) photo of (a) Hg^{2+}-induced hemolysis and (b) inhibition of Hg^{2+}-induced hemolysis by the mesocaptor.

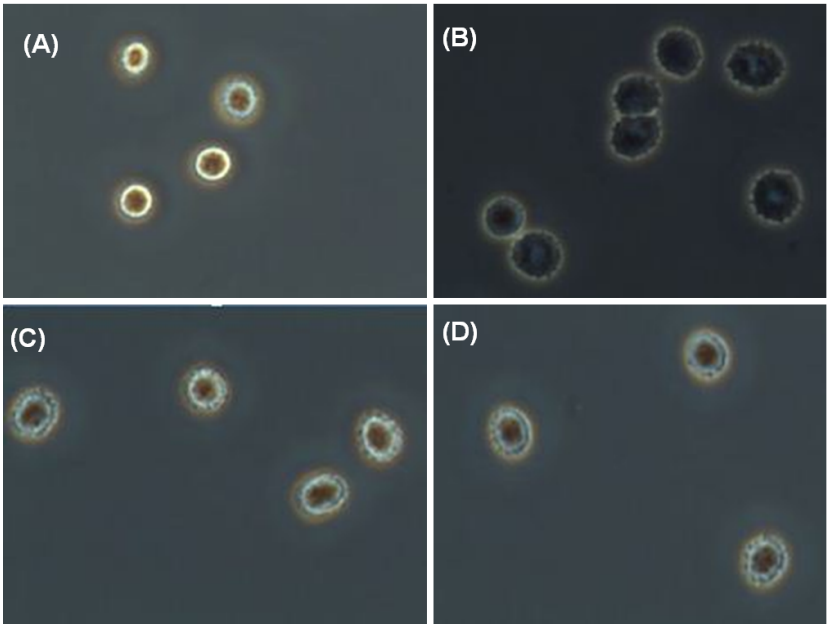

Fig. S13: Phase contrast microscopic images (X 100) showing RBCs: (A) control setup (PBS/H_2O_2 only) incubated for 1 h, (B) Hg^{2+}-induced hemolysis after 1 h of incubation in PBS/H_2O_2, (C) nanosensor addition and inhibition of Hg^{2+}-induced hemolysis after incubation for 1 h, and (D) nanosensor alone (see Attached video). Each sample was analyzed under a phase-contrast microscope (Olympus BX53, Japan). Digital images were taken with a camera (Shimadzu, Japan). *Motic image Pluse 2* was used to process the images.